RESEARCH ARTICLE OPEN ACCESS

Decoupled Control Structure Based Fractional Order PID Controller on the AMB System

Chao-Yun Chen[1], Chia-Juei Fan[2], Wei-Tao Huang[3], Po-Hsiang Tsai[4]
Green Energy and Environment Research Laboratories, Industrial Technology Research Institute, Chutung, Hsinchu, Taiwan.
Email: [1]cychen1022@itri.org.tw, [2]CJFan@itri.org.tw, [3]WTHuang@itri.org.tw, [4]PHTsai@itri.org.tw

Abstract:

This study is concerned with the vibrations of the parallel and conical modes on the high rotation speed shaft supported by the Active magnetic bearings (AMB), the vibrations are mainly due to the gyroscopic effects of the rotating shaft. In order to enhance the stability of the maglev shaft, the physical effects that the parallel and conical modes of the shaft must be decoupled. The conventional integer order PID (IOPID) controller has been integrated popularity into the decoupled control structure because of easily implementation and tuning intuitive. However, the IOPID controller may not be sufficient to stabilize complex dynamics of the AMB system. For the propose of enhancing the stability of the AMB system, this study integrates the fractional order PID (FOPID) controller into the decoupled control structure. In the experiments, the centrifugal compressor equipped with five-degree of freedom AMB is used to evaluate the performance of the FOPID and the experimental results show the performance of FOPID compared with IOPID, in which the FOPID can exhibit satisfactory performance.

Keywords — **Active Magnetic bearing, decoupled control, IOPID, FOPID.**

I. INTRODUCTION

AMB has many advantages compared with the traditional bearings, especially in the non-contact characteristic that improves applicability of AMB supported shaft to the high rotation speed applications such as the maglev centrifugal compressor that has played a key role in the high efficiency chiller of the high-end air-conditioning systems. However, the components of shaft, impeller and disk, that resulted in the gyroscopic effects which lead to the vibrations in the high rotation speed. In the control structure of the AMB system, the decentralized control has fundamental structural deficiencies which lead to the unsatisfactory closed-loop system performance, namely decentralized control cannot solve the problem. Another control structure, decoupled control that can effectively improve the control performance due to the gyroscopic effects, because of the decoupled control has the ability to deal with the parallel and conical vibrations individually using the center of gravity (COG) coordinate transformation, in which the conical vibration was caused by the gyroscopic effects [1].

In pace with advancement of semiconductor process technology, the advanced control theory can be more easily implemented in DSP. Chen et al. applied integral sliding mode control to the three-pole AMB system with assembly error and non-uniform flux distribution [2], Yoon et al. proposed to applied output regulation approach to deal with the rotor unbalance problem of AMB systems [3]. Yoon et al. implemented the LQG control and μ-synthesis to the maglev centrifugal compressor [4]. Although the modern control theory has the ability to deal with the nonlinear phenomenon of the AMB system, however these advanced control approach requires the accurate system modeling technology, and their mathematical method is too complex, even if the advanced control approach has the strongly performance.

In actual industrial applications, the conventional PID controller has gained popularity in AMBs systems because of easily implementation and tuning intuitive [5, 6]. However, the PID controller may not be sufficient to stabilize complex dynamics of AMBs supported rotor. Recently, PID controller have been extended to another expressed form using the all-coefficient adaptive control approach (ACAC). Di et al. applied ACAC to a High-speed

desorption pump supported by AMBs, the ACAC can guarantee the close-loop stability and minimize the vibration during the speed increase as well as at the operational speed [7]. Furthermore, fractional order PID Controller has been developed to the control engineering, FOPID is based on the PID generalized form using fractional calculus [8], Matignon proved the stability results as well as the theory of the controllability and observability of finite-dimensional linear fractional differential systems [9]. Oustaloup was the first to propose the concept of fractional PID controller and successfully used in the CRONE control [10]. Padula proposed the tuning rules for FOPID and the tuning rules allow to minimize the integrated absolute error subject to a constraint on the maximum sensitivity [11]. In actually, a fractional-order system which includes a fractional-order controller, a fractional-order controlled object, and both in practical applications.

According the aforementioned literature reviews, the advanced control approach and real time adaptive control method are not suitable for AMB systems in industrial applications, the reasons included that the actual industrial control products require the strongly reliability and stability. Moreover, the easily maintenance is a critical point for the service engineers. In view of this, FOPID has the advantages that included easily implementation and tuning intuitive, and FOPID can be more closely fit the actual system dynamics. For the propose of enhancing the stability of the AMB system, this study has applied IOPID to integrate the decoupled control, and the high rotation speed shaft supported by AMB is equipped in the centrifugal compressor that is used to evaluate the decoupled control structure based FOPID. Finally, the experimental results show that the FOPID exhibits satisfactory performance compared with the IOPID.

The rest of this paper is organized as follows. Section 2 gives an introduction of the AMB system modeling and the decoupled control structure. Section 3 introduces the IOPID and its implementation. Experimental setup and results are included in Section 4, while conclusions are drawn in Section 5.

II. A BRIEF INTRODUCTIONS OF THE AMB SYSTEM AND DECOUPLED CONTROL STRUCTURE

A rotor equipped with the AMB can be shown in Fig. 1 [1].

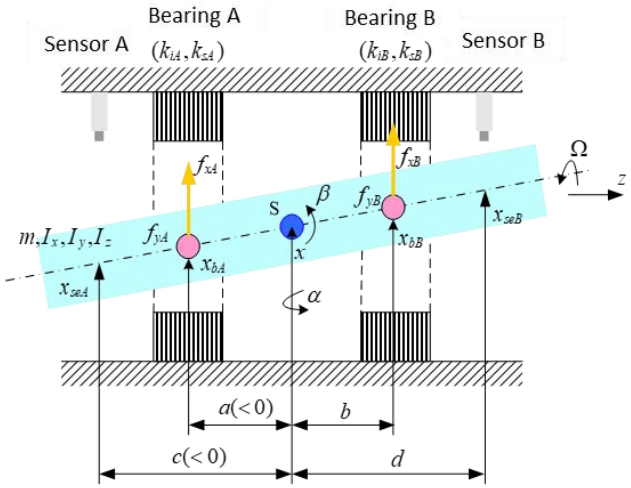

Fig. 1. The AMB rotor model diagram [1].

According to Fig. 1, the center of mass displacements x and y as well as the Euler angles α and β, all combined into the vector q, the measured rotor displacements x_{seA}, x_{seB}, y_{seA}, and y_{seB}, are comprised in the output vector Y. the AMB rotor dynamic equation can be written as below [1]

$$M\ddot{q} + G\dot{q} = Bu_f \quad (1)$$

$$Y = Cq \quad (2)$$

where $M = \begin{bmatrix} I_y & 0 & 0 & 0 \\ 0 & m & 0 & 0 \\ 0 & 0 & I_x & 0 \\ 0 & 0 & 0 & m \end{bmatrix}$, $B = \begin{bmatrix} a & b & 0 & 0 \\ 1 & 1 & 0 & 0 \\ 0 & 0 & a & b \\ 0 & 0 & 1 & 1 \end{bmatrix}$, $G = \begin{bmatrix} 0 & 0 & I_z\Omega & 0 \\ 0 & 0 & 0 & 0 \\ -I_z\Omega & 0 & 0 & 0 \\ 0 & 0 & 0 & 0 \end{bmatrix}$, $C = \begin{bmatrix} c & 1 & 0 & 0 \\ d & 1 & 0 & 0 \\ 0 & 0 & c & 1 \\ 0 & 0 & d & 1 \end{bmatrix}$, $q = (\beta, x, -\alpha, y)^T$, $u_f = (f_{xA}, f_{xB}, f_{yA}, f_{yB})^T$, $Y = (x_{seA}, x_{seB}, y_{seA}, y_{seB})^T$. The magnetic bearing force u_f can be described as

$$u_f = \begin{bmatrix} f_{xA} \\ f_{xB} \\ f_{yA} \\ f_{yB} \end{bmatrix} = - \begin{bmatrix} k_{sA} & 0 & 0 & 0 \\ 0 & k_{sB} & 0 & 0 \\ 0 & 0 & k_{sA} & 0 \\ 0 & 0 & 0 & k_{sB} \end{bmatrix} \begin{bmatrix} x_{bA} \\ x_{bB} \\ x_{bA} \\ x_{bB} \end{bmatrix}$$

$$+\begin{bmatrix} k_{iA} & 0 & 0 & 0 \\ 0 & k_{iB} & 0 & 0 \\ 0 & 0 & k_{iA} & 0 \\ 0 & 0 & 0 & k_{iB} \end{bmatrix}\begin{bmatrix} i_{xA} \\ i_{xB} \\ i_{xA} \\ i_{xB} \end{bmatrix}$$

$$=-K_s q_b + K_i i \quad (3)$$

where k_s is the displacement stiffness, k_i is the current stiffness, q_b is the displacement of bearing coordinates, and i is the individual coil control currents of AMB.

In the decoupled control structure, the crucial point is to utilize the COG displacements rather than the sensor coordinates by involving the transformation matrix T_{in}, and the transformation matrix T_{out} has been applied for the recomposition of the magnetic bearing forces. According to Fig. 1, the displacement signal must be transformed from sensor coordinates to COG, and the transformed displacement signal represents the parallel and conical modes respectively. The displacement signal q_{COG} of COG can be obtained from Eq.,

$$q = T_{in} q_{se} = \begin{bmatrix} c & 1 & 0 & 0 \\ d & 1 & 0 & 0 \\ 0 & 0 & c & 1 \\ 0 & 0 & d & 1 \end{bmatrix}^{-1} q_{se} \quad (4)$$

where $q_{se} = Y$.

Moreover, transforming the bearing coordinates q_b into the COG coordinates q, the AMB rotor dynamic equation can be rewritten as

$$M\ddot{q} + G\dot{q} + K_{ss} q = BK_i i \quad (5)$$

where $K_{ss} = BK_{ss}B^T$.

Considering the right side of Eq. (5), the control current signal must be transformed into the AMB force, $T_{out} = {K_i}^{-1}B^{-1}$ is used to the transformation, which detailed descriptions can be found in [1], and according to the PID feedback control law, the control current i of Eq. (5) can be expressed as Eq. (6), which represents the control of parallel and conical modes.

$$i =- T_{out} P T_{in} q_{se} - T_{out} I T_{in} \dot{q}_{se} - T_{out} D T_{in} \ddot{q}_{se} \quad (6)$$

where P, I, and D are the diagonal matrix, which is the PID control parameters.

III. Fractional Order PID Controller and its Implementation

A. Fractional order calculus

Fractional, or non-integer order fundamental operator of differentiation and integration is denoted by

$${}_aD_t^\alpha = \begin{cases} \frac{d^\alpha}{dt^\alpha}, & \alpha > 0, \\ 1, & \alpha = 0, \\ \int_a^t (d\tau)^{-\alpha}, & \alpha < 0, \end{cases} \quad (6)$$

where α is the fractional order of the differentiation or integration, and typically $\alpha \in \Re$ but it also can be complex number [12]. This article discusses the case where the fractional order is a real number. And the Riemann-Liouville definition is used to define fractional calculus as follows.

$${}_aD_t^\alpha f(t) = \lim_{h\to 0} \frac{1}{\Gamma(m-\alpha)} \left(\frac{d}{dt}\right)^m \int_0^t \frac{f(\tau)}{(t-\tau)^{1-m+\alpha}} d\tau \quad (7)$$

where $m-1 < \alpha < m$ and $\Gamma(m-\alpha) = \int_0^\infty e^{-t} t^{(m-\alpha)-1} dt$ is Euler's gamma function. After establishing the definitions of fractional order calculus, the formula for the Laplace transform of the derivative of order α has been discussed. It is shown in [13] that the Laplace transform of an α, the derivative of signal $x(t)$ is given by

$$L\{D^\alpha x(t)\} = \int_0^\infty e^{-st} \, {}_0D_t^\alpha x(t) dt$$

$$= s^\alpha X(s) - \sum_{k=0}^{m-1} s^k \, {}_0D_t^{\alpha-k-1} x(t)|t = 0 \quad (8)$$

A fractional order differential equation can be expressed in a transfer function form which it provided both the input and output signal as fallow

$$G(s) = \frac{a_1 s^{\alpha 1} + a_2 s^{\alpha 2} + \cdots + a_m s^{\alpha m}}{b_1 s^{\beta 1} + b_2 s^{\beta 2} + \cdots + b_m s^{\beta m}} \quad (9)$$

B. Fractional order transfer function approximation algorithm and its implementation

Oustaloup [10] presented an approximation algorithm which can fit the fractional order operator to a bank of integer order filters in the specified frequency band. The fractional order α in the specified frequency band $[\omega_l, \omega_h]$ is given as follows

$$s^\alpha = (\omega_h)^\alpha \prod_{k=1}^{N} \frac{s+\omega_k'}{s+\omega_k}, \quad 0 < \alpha < 1 \quad (10)$$

where N is the number of poles and zeros which are evaluated as $\omega_k' = \omega_l(\omega_h/\omega_l)^{2k-1-\alpha/2N}$ and $\omega_k' =$

$\omega_l(\omega_h/\omega_l)^{2k-1+\alpha/2N}$. For the case α<0, the Eq. (10) would be inverted. For the case $|\alpha|$>1, s^α should be rearranged to $s^\alpha = s^n s^\sigma$ .Where n is an integer number and $\sigma \in [0,1]$, s^σ term needs to be approximated by Eq. (10).

Bilinear transformation is the IIR filter design technology used in this article. The s-domain transfer function, H(s), is mapped to the z-domain through Eq. (11) to become the transfer function, H(z). For implementation, The H(z) needs to be sorted into Eq. (12). There will be no spectrum aliasing problem regardless of the original s-domain transfer function and bandwidth. After bilinear transformation, the amplitude frequency response range will not exceed half of the sampling frequency, fs. Even if there is no spectral aliasing problem in bilinear transformation, the input data must satisfy the sampling theorem. If the original input data is under sampled due to a low sampling frequency and violates the sampling theorem, then any filter cannot eliminate the errors caused by under sampling. However, it must be noted that there will be nonlinear distortion with the original s-domain frequency after bilinear transformation conversion, and the frequency distortion effect will be more apparent as it approaches half of the sampling frequency.

$$s = \frac{2}{T_s}\left(\frac{1-z^{-1}}{1+z^{-1}}\right) \tag{11}$$

$$H(z) = \frac{\sum_{k=0}^{N} b(k)z^{-k}}{1-\sum_{k=1}^{M} a(k)z^{-k}} \tag{12}$$

where Ts is the sampling period and z is a complex number.

In order to implement the differential equation in digital signal processor, the digital filter uses Direct-Form I [14]. While there are many variants of this type of filter structure, the Direct-Form I method is considered to have the best performance against filter coefficient quantization errors and stability problems, and is also the method used in this article. To balance the performance of the fractional order PID with the difficulty of DSP implementation, the number of poles and zeros N is set to 5, and the frequency limits ω_l and ω_h to 0.1 and 50,000 respectively. However, since the system order is still high, the filter poles and zeros in the direct structure are very sensitive to various errors in the filter coefficients. For instance, quantization errors in the coefficients can cause the filter poles and zeros to move on the z plane, leading to amplitude frequency response that fails to meet the requirements. Additionally, rounding errors may accumulate with the number of operations, leading to filter instability, while overflow errors can cause the filter to oscillate. Fortunately, JTAG (Joint Test Action Group) can confirm the DSP variables of the embedded system in real-time, allowing for the detection of overflow errors quickly.

During the practice, it was found that the simulated filter coefficients were stable during computer analysis but unstable during DSP implementation. The instability of the control system caused by such filter coefficients was resolved by changing single-precision floating-point numbers to double-precision floating-point numbers. At the same time, the possibility of overflow errors in numerical calculations is reduced. In addition to consuming more memory space, changing from single-precision floating-point numbers to double-precision floating-point numbers posed a main difficulty, which was that the DSP floating-point arithmetic unit in used was FPU32, which could only calculate 32-bit floating-point numbers. Therefore, the operation of 64-bit double-precision floating-point numbers could not be effectively accelerated. The AMB control involves the control of five degrees of freedom. With the decoupling architecture, it includes the translational, inclination displacements of the radial X-Y axis, and axial position control. Each degree of freedom has a corresponding fractional order PID controller. In addition to the AMB controller, the control system also includes several filters for suppressing position and current signal noise and AMB system resonance. Besides, a serial communication interface program is in operation to monitor the AMB trajectory on a personal computer. Due to limited DSP resources, the AMB position control loop in this article is choose as 3kHz. To fully utilize the performance of fractional order PID controller in five degrees of freedom AMB control system, a DSP with a 64-bit double-precision f floating-point arithmetic unit is necessary and crucial.

IV. EXPERIMENTAL SETUP AND RESULTS

A. Experimental Setup

The hardware of the experimental system, which is shown in Fig. 2, consists of a centrifugal compressor equipped with five degrees of freedom AMBs. Its composition includes an impeller, an induction motor, a rotor, two radial AMBs, one axial AMB, inductive-type sensors, a variable-frequency drive, and a magnetic bearing drive controller. The magnetic bearing drive controller, which includes a drive circuit, a DSP-based control circuit, and a sensor circuit, is embedded on the side of the centrifugal compressor. The sensor circuit provides five-degree of freedom position feedback and pulse signal of rotor rotation. The magnetic centrifugal compressor is used to evaluate the performance of FOPID controller, which had implemented by digital signal processor, TI-TMS320F28335. The fractional order setting of FOPID derivative term is 0.97 and N=5.

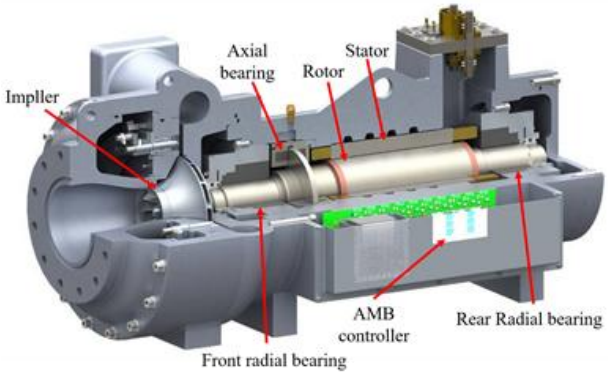

(a)

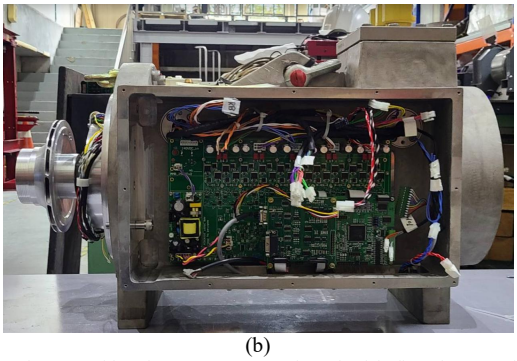

(b)

Fig. 2. Maglev centrifugal compressor equipped with five-degree of freedom AMBs. (a) The sturcure of the rotor supported by AMB. (b) Maglev centrifugal compressor equipped with the AMB drive controller

B. Experimental results

1) ***Experiment #1: The performance of the external disturbance rejection between FOPID and IOPID***

Owing to the theoretical analysis of the FOPID that has the better control performance compared with the IOPID in the complex dynamics, and the maglev centrifugal compressor of this experiment will be equipped with the chiller in the air conditioning application, in which the refrigerant fluid can be regarded as the external disturbance in the AMB system, and the disturbance of refrigerant fluid is not constant. In order to verify the feasibility of FOPID compared with the traditional IOPID in the practical applications, the $0.016\sin(2\pi ft)$ is used as the sine sweep to simulate the external disturbance, in which f=1~1kHz.

Fig. 3 indicate the measured displacement response of the x-axis in the front AMB, the max value of the peak-to-peak is 129.4mV using the IOPID, the maximum value of the peak-to-peak is 94mV using the FOPID. From the obtained result, the FOPID exhibits the better performance of the external disturbance rejection than the IOPID.

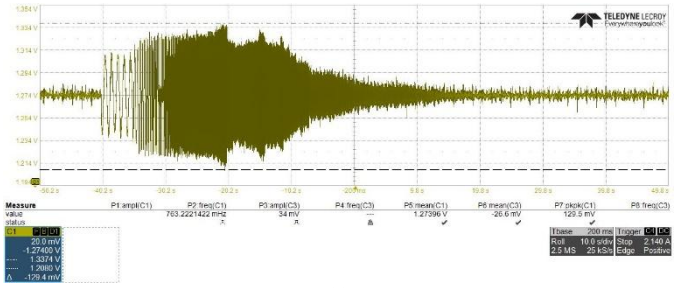

(a)

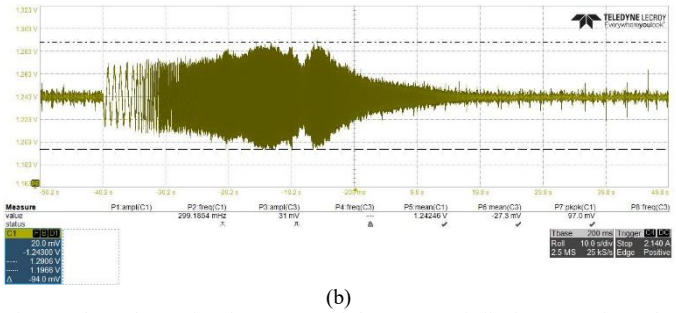

(b)

Fig. 3. The voltage signal response of the measured displacement from the sensor. (a) IOPID. (b) FOPID.

2) ***Experiment #2: The rotor levitation verification of FOPID***

Fig. 4 shows the rotor levitation result using FOPID, the black circle is the backup bearing

clearance, the red dashed circle is the 30% of the backup bearing clearance from international standard (ISO-14839-2) [15]. According to the results of Fig. 3, both the front radial orbit and the rear radial orbit can be precisely controlled in the center of the backup bearing clearance, the maximum vibration percentages are 0.339% and 0.579%, the RMS percentages of orbit are 0.13% and 0.199%. From the vibration of the trajectory, FOPID demonstrates sufficient stability.

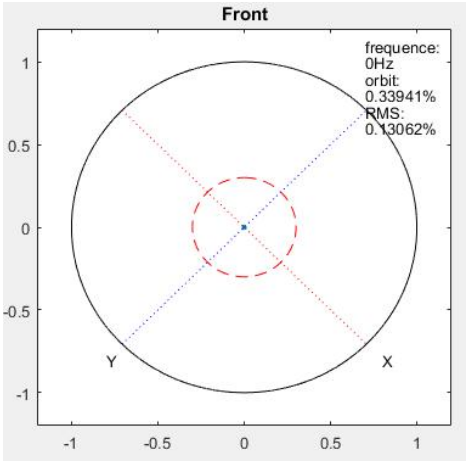

(a)

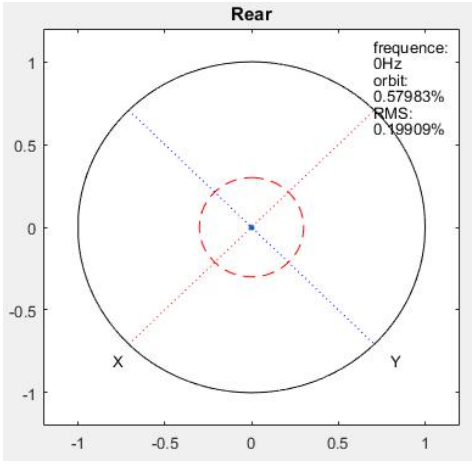

(b)

Fig. 4. The measured rotor orbit of the levitation verification.

3) *Experiment #3: Rotor rotated motion for evaluating the performance compared with the IOPID and FOPID*

Figs. 5 and 6 show the measured rotor orbit of the centrifugal compressor at 9,000rpm (150Hz) using the IOPID and FOPID, respectively. The black circle is the backup bearing clearance, the red dashed circle is the 30% of the backup bearing clearance (ISO-14839-2) [15]. The max vibration percentages of IOPID are 6.915% and 6.236%, and the max vibration percentages of FOPID are 5.034% and 4.85%. Clearly, The FOPID exhibits satisfactory performance compared with the IOPID.

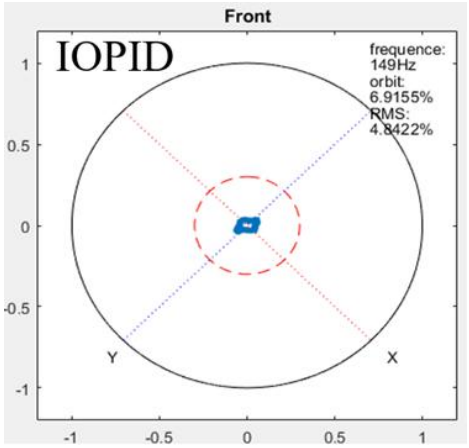

(a)

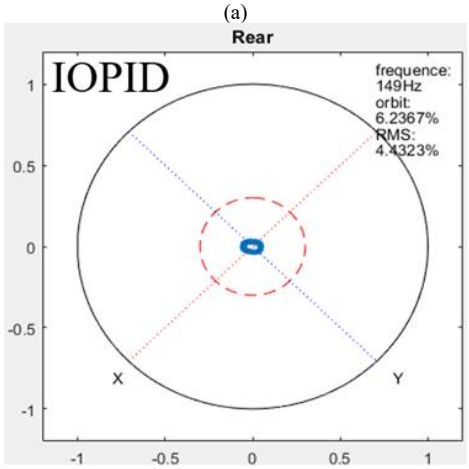

(b)

Fig. 5. The measured rotor orbit of the centrifugal compressor at 9,000rpm using IOPID.

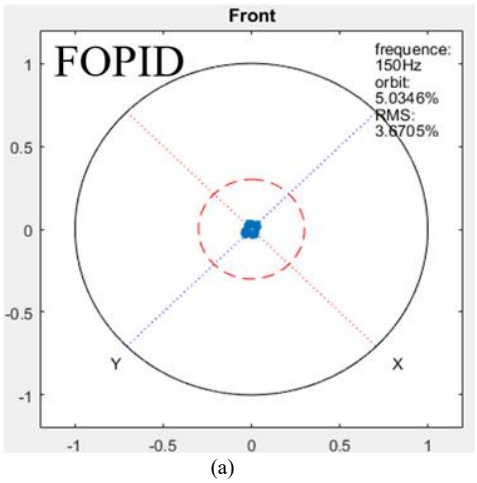

(a)

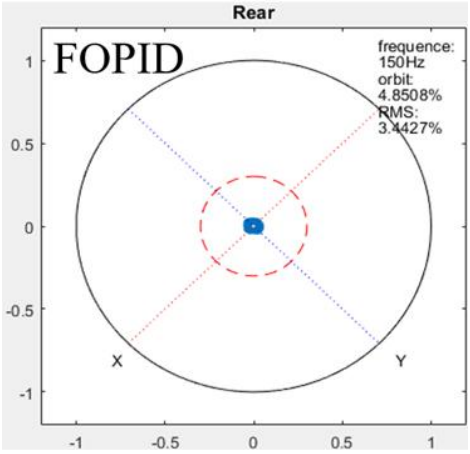

(b)

Fig. 6. The measured rotor orbit of the centrifugal compressor at 9,000rpm using FOPID.

V. CONCLUSIONS

This study applied FOPID to the magnetic centrifugal compressor, the advantages of FOPID are that the controller can be more closely fit the actual system dynamics, easily implementation and tuning intuitive. The fractional order transfer function approximation algorithm and its discretization implementation are described in detail, including the difficulties encountered and the corresponding solutions. The experimental results show that the rotor supported by AMB can be precisely positioned at the center of the backup bearing. In addition, the FOPID controller exhibits superior performance compared with the IOPID controller at the external disturbance rejection and the high rotation speeds.

ACKNOWLEDGMENT

The author would like to thank the Energy Administration, Ministry of Economic Affairs, Taiwan, R.O.C., for supporting this research.

REFERENCES

1. *G. Schweitzer and E. H. Maslen, Magnetic bearing, Springer-Verlag Ber. Heidelberg, 2009.*
2. *S. L. Che, Y. T. Lin, and C. Y. Chen, "Effects of Imperfect Assembly and Magnetic Properties on the Three-Pole AMB System," Applied Science, vol 13, no. 347, pp. 1-11, 2024.*
3. *S. Y. Yoon, L. Di, and Z. Lin, "Unbalance compensation for AMB systems with input delay: An output regulation approach," Control Engineering Practice, vol. 46, pp.166-175, 2016.*
4. *S.Y. Yoon, Z. Lin, and P.E. Allaire, Control of surge in centrifugal compressors by active magnetic bearings: Theory and implementation, Springer Science and Business Media, 2012.*
5. *G. A. Hassaan, "Cointrol of Boiler-drum water level using PID, PD-PI, PI-PD and 2DOF controllers, " International Journal of Engineering and Techniques, vol. 10, no. 1, IJET-V10I1P3, 2024.*
6. *Md Mahmud, S. M. A. Motakabber, A. H. M. Zahirul Alam, and A. N. Nordin, "Control BLDC motor speed using PID controller, International Journal of Advanced Comuputer Science and Applicatiohns, vol. 11, no., 3, pp. 447-481, 2020.*
7. *L. Di, C. Y. Chen, C. H. Lin, and Z. Lin, "Characteristic Model Based All-Coefficient Adaptive Control of a High-Speed Desorption Pump Supported by AMBs,". 15th international Symposium on Magnetic Bearings, 3-6 Aug. 2016, T2B4.*
8. *I. Podlubny, Fractional Differential Equations, New York, NY, USA: Academic Press, 19699.*
9. *D. Matignon and B. D'Andrea-Novel, "Observer-based controllers for fractional differential systans," In: 36th IEEE conference on Decision and Control, San Diego,California, 10-12 December 1997, pp.4967–4972.*
10. *A. Oustaloup and B. Mathieu, La commande CRONE: Du scalaire au multivariate. Paris, France: Hermes, 1999.*
11. *F. Padula and A. Visioli, "Tuning rules for optimal PID and fractional-order PID controllers. Journal of Process Control, vol. 21, no. 1, pp. 69-81, 2011.*
12. *A. Oustaloup, F. Levron, B. Mathieu, and F.M. Nanot FM, "quencyband complex noninteger differentiator: characterization and synthesis," IEEE Trans. Circuits and Systems I, vol. 47, no. 1, pp. 25–39, 2000.*
13. *I. Podlubny, The Laplace Transform Method for Linear Differential Equations of the Fractional Order, PhD Thesis, Technical University of Kosice, Slovak, 1997.*
14. *A. V. Oppenheim and R. W. Schafer, Digital Signal Processing. Englewood Cliffs, NJ: Prentice-Hall, 1975.*
15. *ISO 14839-2: Mechanical vibration - Vibration of rotating machinery equipped with active magnetic bearings - Part 2: Evaluation of vibration, 2004.*